



**HAL**  
open science

## First successful stabilization of consolidated amorphous calcium phosphate (ACP) by cold sintering: toward highly-resorbable reactive bioceramics

Marina Luginina, Roberto Orru, Giacomo Cao, David Grossin, Fabien Brouillet, Geoffroy Chevallier, Carole Thouron, Christophe Christophe Drouet

### ► To cite this version:

Marina Luginina, Roberto Orru, Giacomo Cao, David Grossin, Fabien Brouillet, et al.. First successful stabilization of consolidated amorphous calcium phosphate (ACP) by cold sintering: toward highly-resorbable reactive bioceramics. *Journal of materials chemistry B*, 2020, 8 (4), pp.629 - 635. 10.1039/c9tb02121c . hal-02505112v1

**HAL Id: hal-02505112**

**<https://hal.science/hal-02505112v1>**

Submitted on 7 Jan 2021 (v1), last revised 11 Mar 2020 (v2)

**HAL** is a multi-disciplinary open access archive for the deposit and dissemination of scientific research documents, whether they are published or not. The documents may come from teaching and research institutions in France or abroad, or from public or private research centers.

L'archive ouverte pluridisciplinaire **HAL**, est destinée au dépôt et à la diffusion de documents scientifiques de niveau recherche, publiés ou non, émanant des établissements d'enseignement et de recherche français ou étrangers, des laboratoires publics ou privés.

# First successful stabilization of consolidated Amorphous Calcium Phosphate (ACP) by cold sintering: toward highly-resorbable reactive bioceramics

Marina Luginina,<sup>a,b</sup> Roberto Orru,<sup>\*a</sup> Giacomo Cao,<sup>a</sup> David Grossin,<sup>b</sup> Fabien Brouillet,<sup>b</sup> Geoffroy Chevallier,<sup>b,c</sup> Carole Thouron,<sup>b</sup> Christophe Drouet<sup>\*b</sup>

## Abstract:

In the field of bone regeneration, some clinical conditions require highly-resorbable, reactive bone substitutes to rapidly initiate tissue neo-formation. In this view, Amorphous Calcium Phosphates (ACP) appear as well suited bioceramics taking into account their high metastability. However, the metastability also leads to difficulties of sintering without transformation into crystalline compounds. In this work, various calcium phosphate samples (co)doped with carbonate ( $\text{CO}_3^{2-}$ ) and magnesium ions were synthesized by the double decomposition method in alkaline media using ammonium and potassium hydroxide solutions. The obtained amorphous powders possess an exceptionally-high carbonate content up to 18.3 wt.%. Spark Plasma Sintering (SPS) at very low temperature ( $150^\circ\text{C}$ ) was then utilized to consolidate initial powders with the view to preserve their amorphous character. The influence of the introduction of different apatite growth inhibitors such as carbonate ( $\text{CO}_3^{2-}$ ) and magnesium ions was studied. XRD and FTIR analysis revealed that sintered ceramics generally consisted in highly carbonated low-crystallinity apatites, which are expected to have higher solubility than conventional apatite-based systems. However, most interestingly, modulation of the doping conditions allowed us to retain, for the first time, the amorphous character of ACP powders after SPS. Such consolidated ACP compounds may now be considered as a new family of bioceramics with high metastability allowing the fast release of bioactive ions upon resorption

## Introduction

In the past decades, the development of synthetic calcium-phosphate-based bioceramics as alternative approach for allograft and autograft tissue replacement has been a major subject of research<sup>1-3</sup>. Hydroxyapatite (HAp), ( $\text{Ca}_{10}(\text{PO}_4)_6(\text{OH})_2$ ), due to its good biocompatibility and structural similarity to the mineral part of calcified tissues, is one of the most commonly used bioactive ceramics as of today<sup>4</sup>. However, it is thermodynamically stable under physiological conditions and thus exhibits a low resorption rate *in vivo*. Additionally, due to the low surface area and limited surface reactivity HAp bioactivity is hindered after implantation<sup>5,6</sup>. Such differences with respect to bone mineral, also called biological apatite, are ascribed to the fact that the latter consists of nanocrystalline non-stoichiometric polysubstituted apatite<sup>7</sup>. Besides carbonate ( $\text{CO}_3^{2-}$ ), which is the main substituting ionic group in biological apatite (5-9 wt.%)<sup>8-10</sup>, other ions such as  $\text{HPO}_4^{2-}$ ,  $\text{Mg}^{2+}$ ,  $\text{Sr}^{2+}$ ,  $\text{Na}^+$  and  $\text{F}^-$  are also encountered<sup>11,12</sup>. According to Legros et al.<sup>13</sup>, the composition of bone mineral is characterized by significant vacancy contents in Ca and OH sites, and can be described (omitting trace elements) by the general formula  $\text{Ca}_{8.3}(\text{PO}_4)_{4.3}(\text{CO}_3, \text{HPO}_4)_{1.7}(\text{CO}_3, \text{OH})_{0.3}$ . A recent report analyzing a fresh bone specimen by NMR and vibrational spectroscopies pointed in particular to a high amount of  $\text{HPO}_4^{2-}$  ions besides carbonates<sup>14</sup>. In apatites, whether biological or synthetic, hydroxide ( $\text{OH}^-$ ) and phosphate ( $\text{PO}_4^{3-}$  or  $\text{HPO}_4^{2-}$ ) ionic groups can indeed be replaced by carbonate ions, leading respectively to A and B-type carbonated apatites. Additionally, AB mixed-type apatites are often reported<sup>15</sup>. One important feature of nanocrystalline apatites, whether in bone or dentine or their synthetic

biomimetic analogs, is the presence of a hydrated non-apatitic ionic layer covering the surface of the nanocrystals and conferring very reactive properties<sup>16,17</sup>. In bone, this is used for maintaining ion homeostasis in body fluids, and in synthetic analogs these characteristics can be tailored and exploited to modulate the reactivity/bioactivity of the nanocrystals in view of a variety of biomedical applications, like bone regeneration but also nanomedicine<sup>18,19</sup>. This may also imply ionic substitutions to modulate the bioactivity of the nanocrystals, which may be achieved either for impacting the stability / degree of crystallinity / thermodynamic properties of the apatitic phase<sup>18</sup>, or for modulating biological properties, or both. For example, doping with Mg<sup>2+</sup> ions can activate osteoblast cells, and Mg-doped apatites also exhibit a less pronounced crystallinity (lower maturation state) than Mg-free ones, thus leading to a higher reactivity. Like magnesium, carbonate ions are also growth inhibitors for the apatite structure, having also an impact on apatite nanocrystals reactivity/solubility<sup>20</sup>.

These substitutions and subsequent structural disorder provide thus a way to prepare biomaterials with a higher solubility compared to stoichiometric hydroxyapatite, which may be particularly appealing to rapidly confer constitutive building blocks of mineral in view of activated bone regrowth.

Although the mechanisms of bone mineralization have not yet been fully clarified, it was suggested that the formation of new bone may involve amorphous calcium phosphate (ACP) reactive precursors<sup>21-23</sup>. Such ACP are not crystallized but possess short-range order in the form of small organized units with average size of about 0.9 nm, known as Posner's clusters of chemical formula Ca<sub>9</sub>(PO<sub>4</sub>)<sub>6</sub>.nH<sub>2</sub>O<sup>24</sup>. Despite the relevance of ACP to the field of bone regeneration, these amorphous compounds have not found as yet the development they deserve – except as an ingredient in bone cement formulation<sup>25,26</sup>. This can probably be linked to the difficulty to process ACP to make granules or 3D pieces while avoiding their crystallization into crystallized CaP such as apatite. Two main techniques have been proposed so far to obtain synthetic ACP, i.e. a wet route in aqueous medium<sup>27,28</sup> and a dry method carried out at high temperatures<sup>29</sup>. The consolidation of ACP represents a difficult goal to achieve due to the thermal instability of this amorphous precursor. Therefore, relatively mild conditions are required to consolidate it while preserving its metastable character. Overcoming this challenge could then provide a new family of CaP compounds with even greater reactivity and bioresorbability (resorbability *in vivo* being directly related to solubility<sup>3</sup>).

Since years 2000s, the use of Spark Plasma Sintering (SPS) at very low temperature (150°C) was reported to be effective for the consolidation of biomimetic nanocrystalline apatite powders<sup>30-32</sup>, opening the way to as “cold sintering” approaches exploiting the water contained in the compounds. These initial experiments were performed on non-carbonated apatites. More recently, the possibility to adjoin natural polymers such as cellulose fibers to obtain reinforced biomimetic apatite/polymer composites has also been demonstrated<sup>33</sup>. In addition, this low temperature SPS exploration has been extended to the obtainment of carbonated apatites<sup>34</sup>.

The SPS technique is based on the application of a uniaxial mechanical pressure simultaneously with a pulsed current, which causes heating by Joule effect through the electrically conductive die<sup>35</sup>. This method allows consolidating different types of materials including ceramics, metals and polymers under lower temperatures than those usually employed in conventional hot pressing techniques. Despite the possibilities of SPS, very few reports have been focused on cold sintering. Sintering at very low temperature (< 300°C) was yet found to be especially relevant for consolidating biomimetic apatites so as to preserve their nanocrystalline, hydrated and thermodynamically metastable features<sup>32</sup>.

In this light, the goal of this study was to investigate the consolidation ability by SPS at low temperature, of amorphous CaP compounds, with the general aim of producing ACP-based highly reactive and resorbable biomaterials as a novel family of bone substitutes. All previous attempts to stabilize ACP after sintering, including by SPS at low temperature<sup>34</sup>, have failed since the crystallization into apatite was systematically observed. This may be related to several factors such as inadequate synthesis protocols or too low carbonate contents, thus not playing fully their crystallization inhibition role.

In the present work, we have explored alternative synthesis routes to prepare very highly carbonated ACP powder precursors, eventually also containing magnesium ions, so as to allow stabilizing/retaining the amorphous character even after SPS consolidation. Indeed, carbonate and magnesium ions are two crystallization inhibitors for the apatitic structure, but their effect

on low temperature sintering had not been investigated so far. We show here, for the first time, the possibility to obtain still-amorphous compounds, in this case calcium phosphates, after SPS treatment via “low temperature sintering”. This new family of compounds is intended to allow the preparation of highly resorbable CaP ceramics for very fast release of bioactive building blocks relevant to bone tissue regeneration. The main physicochemical characteristics of the obtained samples are also investigated in this paper by taking advantage of complementary techniques.

## Experimental

### Synthesis of amorphous (ACP) powders

The synthesis of five types of ACP-based powders was carried out by double decomposition method<sup>36,37</sup>, with and without carbonate and eventually magnesium ions. The starting materials used to this aim are listed in **Table 1**, along with the selected relative amounts.

Sample name (method number)	Composition			
	Solution A		Solution B	
	Molar concentration, mol/L			
	Ca(NO <sub>3</sub> ) <sub>2</sub> ·4H <sub>2</sub> O	Mg(NO <sub>3</sub> ) <sub>2</sub> ·6H <sub>2</sub> O	(NH <sub>4</sub> ) <sub>2</sub> HPO <sub>4</sub>	NaHCO <sub>3</sub>
ACP <sup>27</sup> (1)	0.3*	0	0.13**	0
cACP (1)	0.3*	0	0.65**	0.1**
Mg5-cACP (1)	0.29*	0.017*	0.65**	0.1**
Mg15-cACP (1)	0.26*	0.05*	0.65**	0.1**
Mg30-cACP (1,2)	0.22*	0.1*	0.65**	0.1**

\*Refers to a 1%vol NH<sub>3</sub> aqueous solution.

\*\* Refers to a 2%vol NH<sub>3</sub> aqueous solution.

**Table 1.** Starting reactants used to synthesize amorphous calcium phosphates (ACP).

Two different solutions, indicated as A and B, respectively, were prepared individually by dissolving the precursors in deionized water. The pH of both solutions was adjusted to ~10 (experimental value 9.9). To this purpose, either ammonium hydroxide (NH<sub>4</sub>OH 20%, Fisher Chemical) (method 1) or potassium hydroxide solution (KOH, Fisher Chemical) (method 2) were utilized as mentioned in the text. As explained in the Result and Discussion section, the Mg30-cACP powders were prepared according to both methods. To this purpose, di-ammonium hydrogen phosphate (NH<sub>4</sub>)<sub>2</sub>HPO<sub>4</sub> was also replaced in the initial solution B by di-potassium phosphate (K<sub>2</sub>HPO<sub>4</sub>), in the same proportion, leading to the sample denoted Mg30-cACP-K. To reach pH 9.9, KOH solutions with pH = 13 or 15 were added to solutions A and B, respectively. Solution B containing HPO<sub>4</sub><sup>2-</sup> ions exhibited buffer properties, so that a stronger initial alkaline solution was required to increase its pH. The rest of the synthesis procedure was the same for both methods. In each case, solution A was added to solution B at room temperature (~22°C). The resulting mixture was stirred for few minutes and then immediately filtered on a Buchner

funnel, washed with alkalinized deionized water (pH 9.9) and freeze-dried. Pure ACP powder was prepared as a reference using the method described by Heughebaert<sup>27</sup>.

### Spark Plasma Sintering (SPS)

SPS experiments for the consolidation of amorphous precursors were carried out by means of a 2080 Sumitomo Coal Mining equipment under argon atmosphere. This equipment provides uniaxial pressing and simultaneous heating via DC pulsed current (maximum 8000 A and 10 V). During the experiments, current was limited to 1000 A, and the sequencing of pulses was 12:2 (12 pulses of 3.3 ms followed by two time intervals without current). Powder samples (0.35 g) were placed in a graphite die with internal diameter equal to 8 mm covered with a graphite foil to facilitate sample release after SPS.

Sintering runs were performed with temperature and pressure programmed sequences (**Figure 1**) similar to

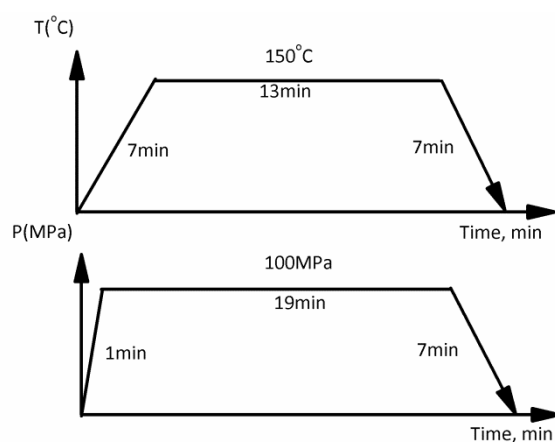


**Figure 1:** SPS conditions (temperature and pressure programs)

those used in a previous studies aimed to the consolidation of biomimetic apatites and derived composites<sup>32,33</sup>.

### Physicochemical characterization

Initial powders and sintered samples obtained after SPS were first characterized by X-ray diffraction, using a BRUKER D8 Advanced diffractometer with CuK $\alpha$  radiation. XRD spectra were recorded in a range 10–90° with a step size 0.02 and dwell time 1s. In addition, vibrational spectrometry analysis was conducted on a Nicolet 5700 Fourier transform infrared (FTIR) spectrometer. Spectra were recorded in transmission mode in the 400–4000 cm<sup>-1</sup> range with 64 scans and 4 cm<sup>-1</sup> resolution, the KBr pellet method was used. Obtained FTIR spectra were analyzed using the OMNIC software (Thermo Fisher Scientific). Ca<sup>2+</sup> and Mg<sup>2+</sup> titrations were carried out by atomic absorption spectroscopy (AAS, in flame mode) using an Analytik Jena contraAA 300 high-resolution continuum source spectrometer. Mechanical evaluations (determination of the tensile strength  $\sigma$ ) were carried out on the SPS pellets (~ 8 mm diameter and 2 mm height) via diametral compression tests, *aka* Brazilian tests, as previously reported<sup>30</sup> on disk-shape samples not suitable for regular axial compression tests. These measurements were performed using a Hounsfield press (model H25K-S) equipped with a 25 kN force sensor and at a loading speed of 0.5 mm/min.

### Results and Discussion

### Powder synthesis and physicochemical characterization

The first systems considered in this study were synthesized using ammonium hydroxide solution as alkalization medium. XRD patterns of the corresponding powders are shown in **Figure 2**. Standard ACP is shown on **Figure 2a**. All other compounds were precipitated in the presence of carbonate ions, hence the denomination cACP, and with increasing magnesium concentrations. For magnesium contents in the starting powder mixture system equal or less than 15 wt.% (**Figure 2b-d**), corresponding to experimental Mg/(Mg+Ca) molar ratios between 0 and 0.13, our results indicated that no defined peaks could be detected by XRD, confirming the preservation of the amorphous character of these carbonated or non-carbonated “ACP” samples. On the other hand, the XRD pattern of Mg30-cACP (**Figure 2e**) showed, in addition to the broad halo with maximum  $2\theta$  value at around  $30^\circ$ , several other prominent peaks, which are attributed to the presence of a secondary  $\text{NH}_4\text{MgPO}_4 \cdot 6\text{H}_2\text{O}$ , struvite, crystalline phase (ICDD-PDF 01-077-2303).

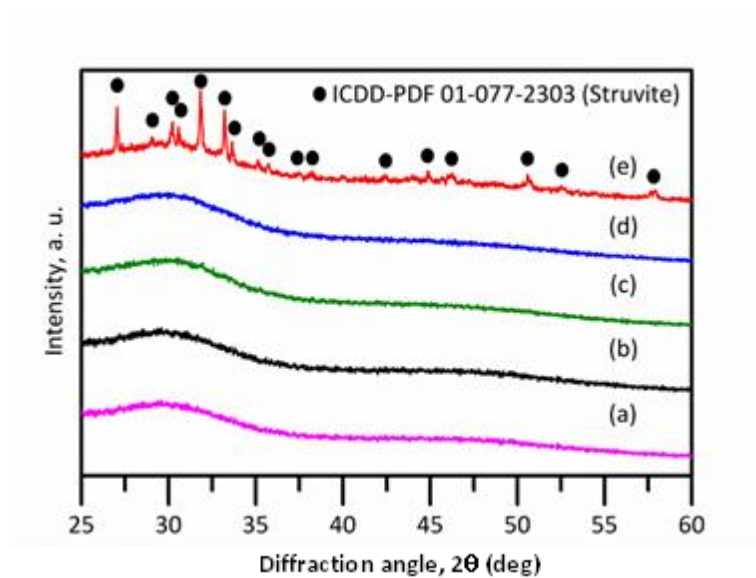


**Figure 2:** Diffraction patterns of powders synthesized using ammonia for pH stabilization: (a) ACP; (b) cACP; (c) Mg5-cACP; (d) Mg15-cACP; (e) Mg30-cACP.

The formation of undesired struvite beyond a limit Mg content may be related to the use of ammonium hydroxide in the synthesis protocol, thus providing the necessary  $\text{NH}_4^+$  ions. Therefore, this biphasic Mg30-cACP sample formed in the presence of  $\text{NH}_4^+$  ions will not be further considered in the study.

FTIR analyses were also recorded for complementary characterization, and the related spectra are presented in **Figure 3**. All the spectra reveal broad bands which are similar to those reported in previous work for ACP obtained by precipitation in an alkaline medium<sup>34,38</sup>. The broad band between  $3700$  and  $2800\text{ cm}^{-1}$  and the one at  $\sim 1640\text{ cm}^{-1}$  can be attributed to the presence of water (respectively O-H stretching and H-O-H bending modes) associated to Posner clusters<sup>39</sup>.

The amorphous character of the samples leads to poorly defined phosphate vibration bands, especially related to the  $\nu_3(\text{PO}_4)$  and  $\nu_4(\text{PO}_4)$  modes, as opposed to observations with other CaP compounds like apatites<sup>40</sup>, and also to a position of the  $\nu_1(\text{PO}_4)$  band close to  $959\text{ cm}^{-1}$  (instead of  $\sim 961\text{--}962\text{ cm}^{-1}$  for apatites)<sup>41</sup>. For carbonated compounds, additional bands assignable to the  $\text{CO}_3^{2-}$  ionic

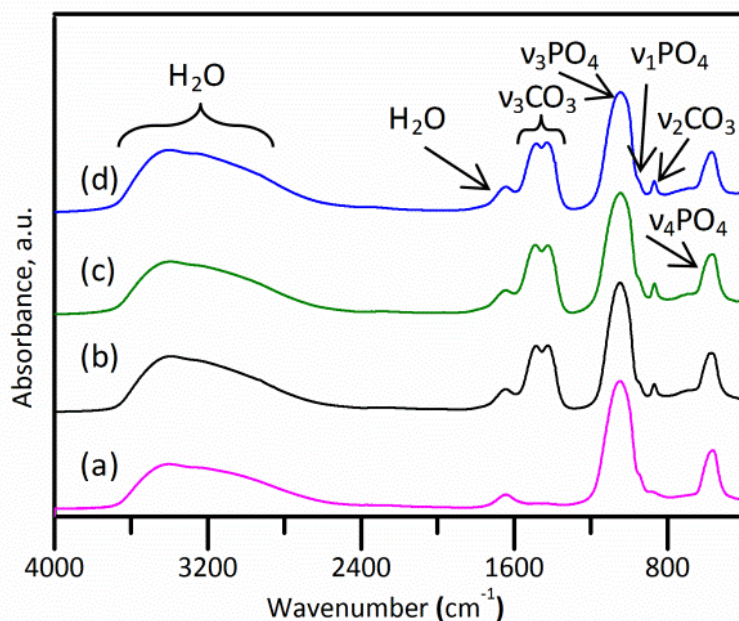


**Figure 3:** FTIR spectra of synthesized powders: (a) ACP; (b) cACP; (c) Mg5-cACP; (d) Mg15-cACP.

group are also detected (**Figure 3**). In particular, typical regions of the spectra where signals of carbonate ions can be observed are  $850\text{--}900\text{ cm}^{-1}$  and  $1350\text{--}1550\text{ cm}^{-1}$ , related to the  $\nu_2(\text{CO}_3)$  and  $\nu_3(\text{CO}_3)$  vibration modes, respectively. Details of these regions are given in **Figure 4(I)** for the cACP synthesized powder. For comparative purposes, the characteristic features of A and B-type carbonate environments in carbonated apatite, respectively corresponding to carbonate ions replacing some hydroxyl and phosphate groups in the apatite structure, have also been pointed out on this figure, and the wavenumbers corresponding to  $\text{CO}_3^{2-}$  ionic groups in nanocrystalline apatites are summarized in **Table 2**. In addition, the estimated position of IR bands corresponding to surface carbonates (i.e.  $\text{CO}_3^{2-}$  ions located on the hydrated layer on apatite nanocrystals)<sup>42,43</sup>, also known as “labile” has also been indicated on **Figure 4** and **Table 2**.

Such labile carbonates are indeed characteristic of metastable chemical environments that may be found in hydrated amorphous domains and not embedded into the crystallographic apatitic structure. It is interesting to note that, in case of this cACP amorphous precursor, carbonate species seem to mostly correspond to such labile  $\text{CO}_3$  (see **Figure 4**), pointing to their similarity to the labile surface carbonates found in the amorphous hydrated layer on nanocrystalline apatites. The same behavior was also observed in the cases of Mg5-cACP and Mg15-cACP initial powders.

The overall content of  $\text{CO}_3^{2-}$  ions was estimated for all samples by exploiting the FTIR features in a quantitative way, according to Grunenwald et al.’s updated methodology<sup>43</sup> (**Table 3**). In particular, the ratio  $r_{c/p}$  between the integrated intensity of  $\nu_3(\text{CO}_3)$  ( $1550\text{--}1350\text{ cm}^{-1}$  domain) and  $\nu_4(\text{PO}_4)$  band ( $1230\text{--}912\text{ cm}^{-1}$ ) was measured and compared to the calibration curve. For the carbonated ACP (cACP), the total amount of  $\text{CO}_3$  was found around 17 wt.%, while for Mg15-cACP it reached 18.3 wt.%. To the best of our knowledge such highly carbonated



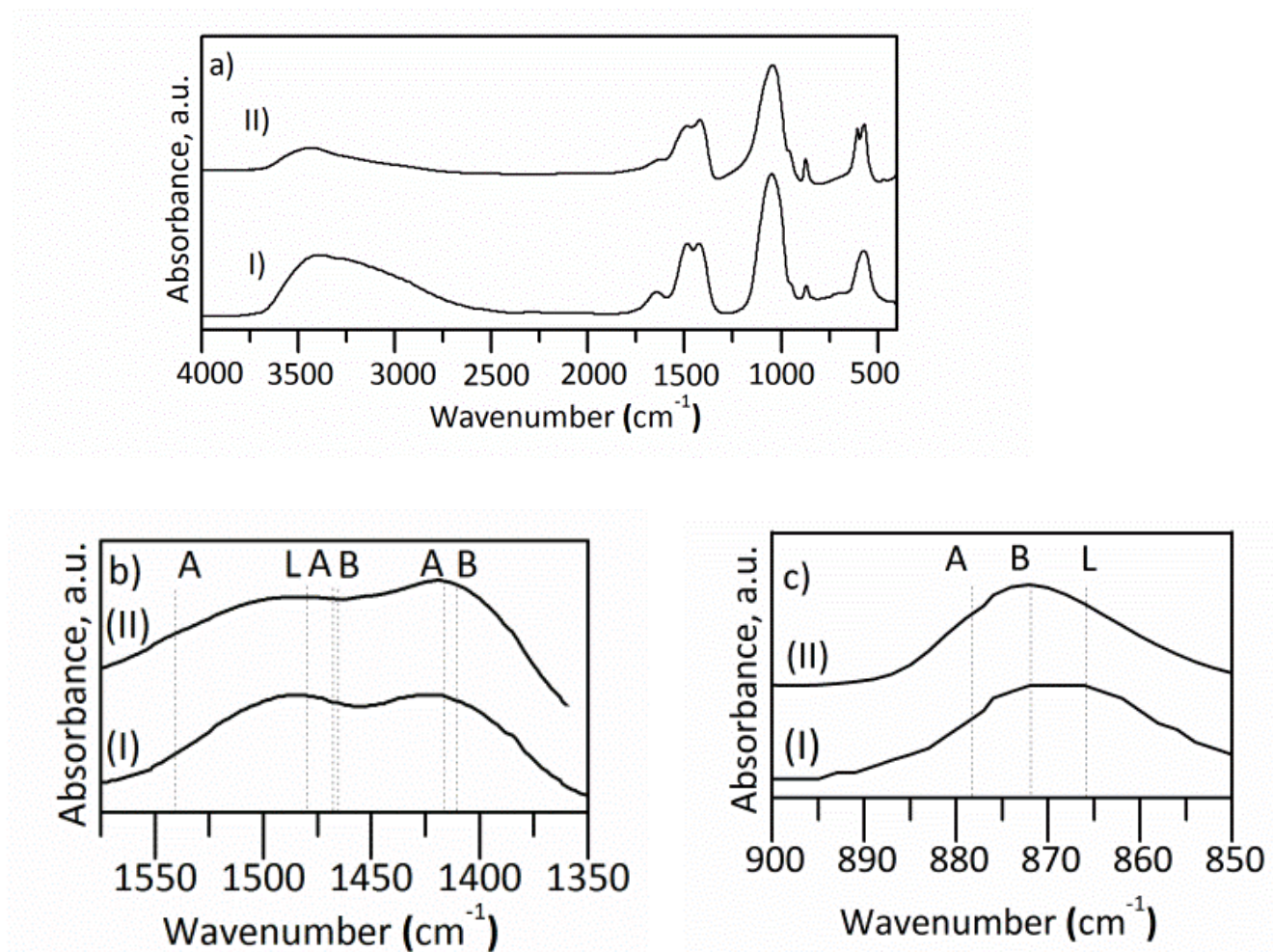


**Figure 4:** FTIR spectra of the cACP powder: (a)(I) initial powder, (a)(II) sample after SPS; (b) zoom on the  $\nu_3(\text{CO}_3)$  band; (c) zoom on the  $\nu_2(\text{CO}_3)$  band. A, B, and L stand respectively for A-type, B-type and Labile carbonates species.

Vibrational band	A-type	B-type	Labile $\text{CO}_3^{2-}$
$\nu_2^{41,44,45}$	882	872	866
$\nu_3^{42,46}$	1465 1542	1412 1462	1417 1480

**Table 2:** Overview of characteristic wavenumbers (in  $\text{cm}^{-1}$ ) of  $\nu_2(\text{CO}_3)$  and  $\nu_3(\text{CO}_3)$  vibration modes in apatites



Name of the sample	CO <sub>3</sub> wt.% Initial powders	CO <sub>3</sub> wt.% Samples after SPS
ACP	0	0
cACP	17.0	14.0
Mg5-cACP	15.9	11.3
Mg15-cACP	18.3	14.1

**Table 3:** Carbonate contents of as-synthesized powders as well as after SPS (evaluated by FTIR; uncertainties estimated to  $\pm 0.5$  wt.%)

amorphous calcium phosphate powders have been synthesized in the present work for the first time. By comparison, amorphous powders with carbonate content reaching around 3.1 wt.% was reported by Ortali et al., although such level was found insufficient to allow preservation of the amorphous character after SPS consolidation<sup>34</sup>. The obtained augmentation of the carbonation level can be explained on the basis of several modifications in the synthesis procedure employed here as compared to literature reports: unheated synthesis (room temperature  $\sim 22^\circ\text{C}$ ), high alkaline pH raised close to 10, high starting C/P ratio  $\sim 1.6$  (as opposed to a maximum of 0.5 in ref. <sup>34</sup>), low starting Ca/P ratio close to 1.1, and absence of precipitate maturation. These conditions thus favor carbonation by providing not only fewer cations and more carbonate ions per unit volume, but also by providing a more stable chemical environment for limiting CO<sub>2</sub> release (high pH, absence of maturation).

In order to avoid the precipitation of Struvite during the synthesis of Mg30-cACP, the preparation of the latter was attempted substituting NH<sub>4</sub>OH by KOH as described in the Materials and Methods section. FTIR spectra of the synthesized powder and the corresponding sample consolidated by SPS are given in **Figure 5a** and **5b**, respectively. The carbonation level of raw Mg30-cACP-K powder was found to be around 13.8 wt.%, while its amorphous character was confirmed by XRD analysis (**Figure 6a**); and its Mg/(Mg+Ca) molar ratio was close to 0.14.

The above data thus allowed us to prepare single-phased, highly carbonated ACP powders, with or without co-incorporation of Mg<sup>2+</sup> ions. The next step therefore consisted of checking their consolidation by low temperature SPS treatment, and to characterize the obtained bioceramic pellets. This is the object of the following section.

### Characterization of Spark Plasma Sintered bioceramics

SPS was tested on each of the carbonated/magnesium ACP compositions prepared (see **Figure 1**). In all cases, successful consolidation was achieved, with the obtainment of hardened pellets. Densification rates (ratio of apparent density to theoretical) of *ca.* 60% were attained for cACP, with a decreasing trend down to *ca.* 45% when increasing the Mg initial content up to 30%. These values point to the residual porosity within the pellets, which can be advantageously exploited for the loading and release of drug/active molecules, also taking into account that the applications aimed with these compounds are not to treat large bone defects in load-bearing sites. Typical values of tensile strength  $\sigma$  evaluated via diametral compression tests reached  $13 \pm 3$  MPa, which are comparable to previous data on CaP compounds (ACP and nanocrystalline apatite) measured in similar conditions<sup>30</sup>. Exploration of the SPS data (Supplementary Information, **Figure S11**) confirmed the occurrence of an actual sintering stage when approaching the 150°C plateau, totally distinct from the powder compression stage noticeable upon applying mechanical pressure.

The XRD pattern of the ceramic obtained from pure ACP (**Figure 7a**) revealed, as anticipated, that crystallization into an apatite phase (ICDD-PDF 00-009-0432) occurred on this sample during SPS. Attempts to avoid this crystallization were then made by investigating the effect of the carbonation and magnesium contents of the amorphous precursor powder. Apatite formation was also

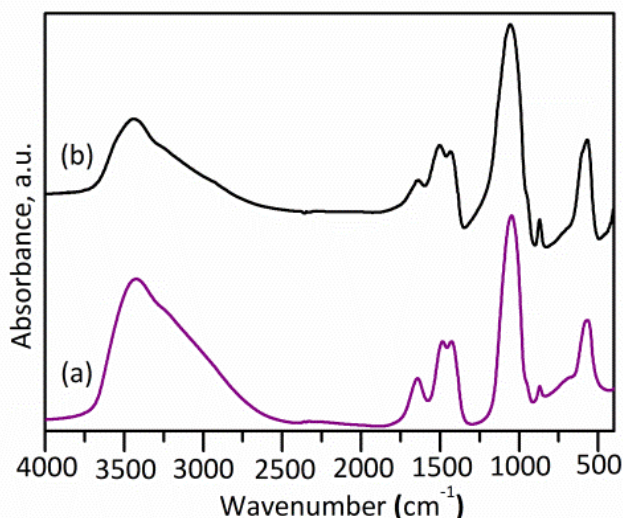


**Figure 5:** FTIR spectra of Mg30-cACP-K synthesized with KOH solution: (a) initial powder; (b) after SPS.

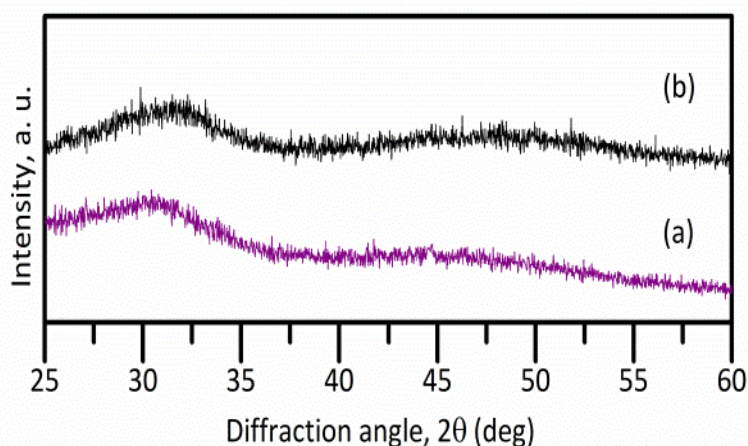


**Figure 6:** XRD patterns of Mg30-cACP-K synthesized with KOH solution: (a) initial powder; (b) after SPS.

noticed for the cases of cACP exempt of magnesium (**Figure 7b**) as well as for low amounts of Mg, namely for samples Mg5-cACP (**Figure 7c**) and Mg15-cACP (**Figure 7d**). However, it may be noted that the related low resolution of the peaks evidences their low crystallinity character (similarly to bone mineral<sup>47</sup>) as opposed to pure ACP. This low crystallinity can be related to several factors as nonstoichiometry, ion substitutions and nanosized crystallites. This tendency toward lower apatite crystallinity is all the more obvious that the Mg content increases (**Figure 7**). It can thus be stated that in these conditions, carbonate and magnesium ions limit, but do not block the progression of apatite crystallization during SPS. This conclusion agrees with previous results reported in the literature<sup>20,48</sup>; however these findings indicate that these starting CO<sub>3</sub>/Mg compositions were not sufficient to stabilize amorphous CaP after SPS.

FTIR spectra also revealed the occurrence of the transformation of amorphous powders into low-crystallinity apatite after SPS treatment for these samples (**Figure 4a-II**). Carbonate ions can

then enter the apatite lattice leading to the formation either A or B-types of substitution. In particular, based on the FTIR spectral analysis, partial transformation into mostly B-type apatite

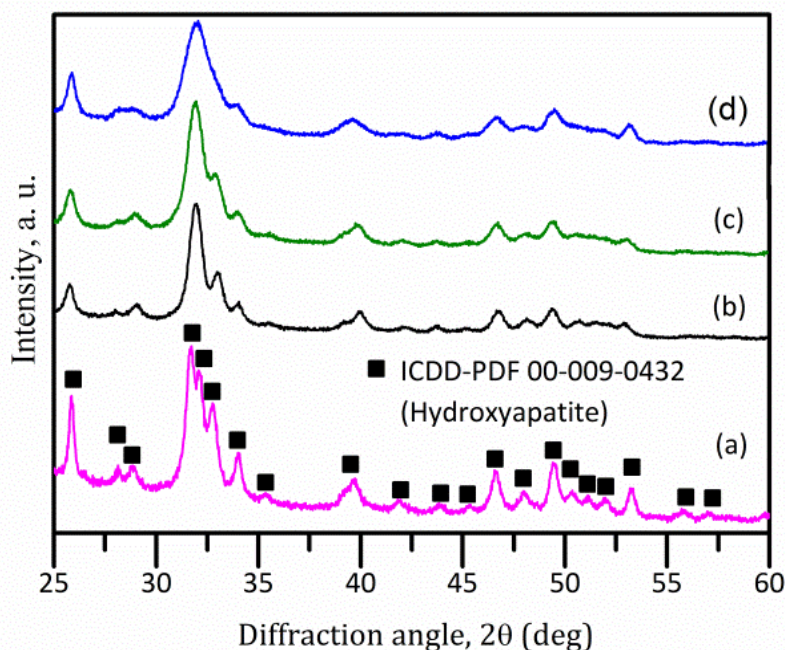


**Figure 7:** Diffraction patterns of the SPS samples obtained from the amorphous powders in presence of ammonium hydroxide solution: (a) ACP; (b) cACP; (c) Mg5-cACP; (d) Mg15-cACP.

can be noted after SPS of these samples in domains  $1462\text{ cm}^{-1}$  (**Figure 4b-II**) and  $872\text{ cm}^{-1}$  (**Figure 4c -II**). FTIR spectra relative to the specimens consolidated by SPS evidenced also a decreasing in the carbonation level (**Table 3**), albeit samples still remained highly carbonated. This diminution can be linked to the partial decomposition of carbonate ions followed by expulsion of  $\text{CO}_2$  gas.

In order to continue our attempts to stabilize ACP even after SPS, greater levels of Mg were tested. SPS treatment at  $150^\circ\text{C}$  was again found to be effective in the consolidation of the sample Mg30-cACP-K synthesized with the KOH solution. However, in this case, the initial amorphous character of calcium phosphate powder could be successfully maintained even after SPS, as confirmed by XRD analysis (**Figure 6b**). To the best of our knowledge, this outcome is obtained for the first time in the literature, thus opening the way for identifying new families of bioceramic/composite materials with high metastability/ surface reactivity/resorption abilities. The preservation of this amorphous state even after SPS is thought to be related to the strong inhibiting effect of the  $\text{Mg}^{2+}$  ions on apatite crystallization combined to that of carbonates. The carbonation level on this sample after SPS was found to be kept around 9 wt.%. The typical morphology of such sintered ACP is shown on **Figure 8**, evidencing in particular a submicron porosity.

The mechanism of sintering at such low temperatures is not fully elucidated. But, similarly to the case of biomimetic apatite nanocrystals which contain water molecules in a surface hydrated layer as well as labile surface ions<sup>30-32</sup>, the presence of water molecules associated to amorphous clusters of ACPs most likely plays a key role in the formation of interparticle bridges resulting in ACP cold sintering. The role of (added) water was also shown to favor sintering (although not via SPS) in the case of crystallized calcium carbonate, when using high pressure compaction<sup>49</sup>. In ACPs, the absence of long-range

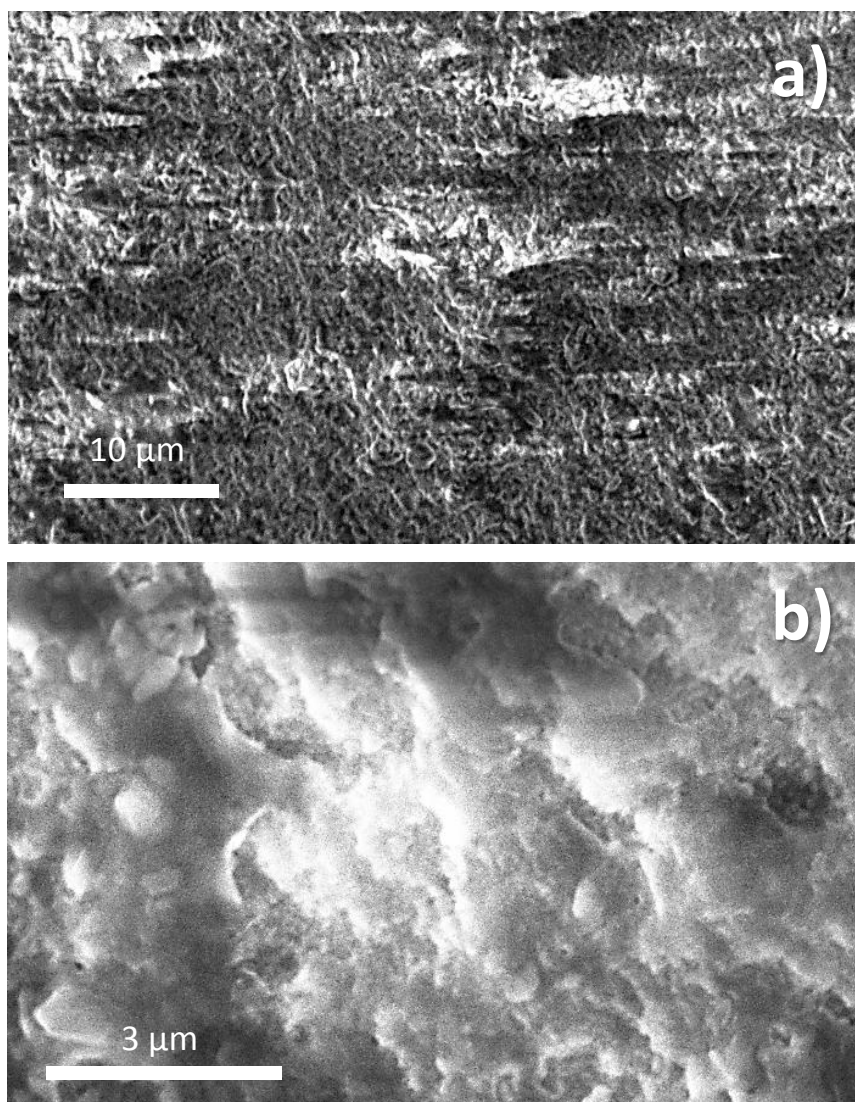


**Figure 8:** SEM micrographs: typical morphology for Mg30-cACP-K samples consolidated by low temperature SPS. Initial magnifications: (a) x2000 and (b) x10000.

order could allow a high mobility of the constitutive ions and H<sub>2</sub>O molecules, which could facilitate ion diffusion despite the low temperature, and thus the consolidation process. The occurrence of dissolution-precipitation on the other hand cannot be, at this stage, neither eliminated nor confirmed in the absence of direct evidence.

## Conclusions

Carbonated and magnesium co-doped amorphous calcium phosphate powders with different compositions were synthesized by an adapted precipitation method and then consolidated by Spark Plasma Sintering at low temperature in view of cold sintering. The high content of carbonate ions was demonstrated (maximum carbonate content  $\sim$  18.3 wt.%). Cold-sintering at 150°C by SPS was effective to consolidate all powders prepared. The influence of the introduction of carbonate and magnesium ions in ACP on the consolidation process was also investigated. The high carbonation (mostly B-type) was preserved after SPS allowing one to expect high resorption rates *in vivo*<sup>50</sup>. Our main finding is the determination of experimental conditions allowing, for the first time, to retain the amorphous nature of ACP compounds system after SPS. Suitable SPS conditions associated to adequate Mg and CO<sub>3</sub><sup>2-</sup>

substitutions are needed to obtain this original outcome. These findings open the way to the development of consolidated ACP-based bioceramics with high (bio)reactivity.

### Conflicts of interest

There are no conflicts to declare.

### Acknowledgements

One of the authors (M.L.) performed her activity in the framework of the International PhD in Innovation Sciences and Technologies at the University of Cagliari, and wishes also to thank the ERASMUS Placedoc program for allowing mobility to France.

### References

- 1 R. Z. LeGeros, *Monogr. Oral Sci.*, 1991, **15**, 1–201.
- 2 S. V. Dorozhkin, *Biomaterials*, 2010, **31**, 1465–1485.
- 3 N. Eliaz and N. Metoki, *Materials (Basel)*, 2017, **10**, 1–104.
- 4 S. Samavedi, A. R. Whittington and A. S. Goldstein, *Acta Biomater.*, 2013, **9**, 8037–8045.
- 5 M. J. Yaszemski, R. G. Payne, W. C. Hayes, R. Langer and A. G. Mikos, *Biomaterials*, 1996, **17**, 175–185.
- 6 J. M. Spivak and A. Hasharoni, *Eur. Spine J.*, 2001, **10**, S197–S204.
- 7 C. Rey, C. Combes, C. Drouet and M. J. Glimcher, *Osteoporos. Int.*, 2009, **20**, 1013–1021.
- 8 J. C. Elliott, D. W. Holcomb and R. A. Young, *Calcif. Tissue Int.*, 1985, **37**, 372–375.
- 9 M. Vallet-Regí and J. M. González-Calbet, *Prog. Solid State Chem.*, 2004, **32**, 1–31.
- 10 R. Z. LeGeros, in *Hydroxyapatite and Related Materials*, ed. B. C. Paul W. Brown, Taylor & Francis Group, Boca Raton, 1st edn., 2017, pp. 3–28.
- 11 S. V. Dorozhkin, *Bioceram. Dev. Appl.*, 2016, **4**, 1–20.
- 12 C. Combes, S. Cazalbou and C. Rey, *Minerals*, 2016, **6**, 1–25.
- 13 R. Legros, N. Balmain and G. Bonel, *Calcif. Tissue Int.*, 1987, **41**, 137–144.
- 14 S. Von Euw, Y. Wang, G. Laurent, C. Drouet, F. Babonneau, N. Nassif and T. Azaïs, *Sci. Rep.*, 2019, **9**, 1–11.
- 15 J. P. Lafon, E. Champion and D. Bernache-Assollant, *J. Eur. Ceram. Soc.*, 2008, **28**, 139–147.
- 16 C. Rey and C. Combes, in *Biomaterialization and Biomaterials: Fundamentals and Applications*, ed. M. P. G. Conrado Aparicio, Woodhead Publishing, Sawston, Cambridge, 1st edn., 2015, pp. 95–128.
- 17 Y. Wang, S. Von Euw, F. M. Fernandes, S. Cassaignon, M. Selmane, G. Laurent, G. Pehau-Arnaudet, C. Coelho, L. Bonhomme-Coury, M. M. Giraud-Guille, F. Babonneau, T. Azaïs and N. Nassif, *Nat. Mater.*, 2013, **12**, 1144–1153.
- 18 C. Rey, C. Combes, C. Drouet, S. Cazalbou, D. Grossin, F. Brouillet and S. Sarda, *Prog. Cryst. Growth Charact. Mater.*, 2014, **60**, 63–73.
- 19 C. Drouet, A. Al-kattan, M. Choimet, A. Tourrette Diallo, V. Santran, J. Dexpert-Ghys, B. Pipy, F. Brouillet and M. Tourbin, *Intern. Med. Prim. Healthc.*, 2015, **1**, 1–9.
- 20 A. A. Campbell, M. LoRe and G. H. Nancollas, *Colloids and Surfaces*, 1991, **54**, 25–31.
- 21 H. A. Lowenstam and S. Weiner, *Science (80- )*, 1985, **227**, 51–53.
- 22 J. Mahamid, B. Aichmayer, E. Shimoni, R. Ziblat, C. Li, S. Siegel, O. Paris, P. Fratzl, S. Weiner and L. Addadi, *Proc. Natl. Acad. Sci. U. S. A.*, 2010, **107**, 6316–6321.

- 23 J. Mahamid, A. Sharir, D. Gur, E. Zelzer, L. Addadi and S. Weiner, *J. Struct. Biol.*, 2011, **174**, 527–535.
- 24 F. Betts and A. S. Posner, *Mater. Res. Bull.*, 1974, **9**, 353–360.
- 25 F. C. M. Dricssens, J. A. Flanell, M. G. Boltong, I. Khairoun and M. P. Ginebra, *Proc. Inst. Mech. Eng. Part H J. Eng. Med.*, 1998, **212**, 427–435.
- 26 A. Tofighi, S. Mounic, P. Chakravarthy, C. Rey and D. Lee, *Key Eng. Mater.*, 2001, **192–195**, 769–772.
- 27 J. C. Heughebaert, Institut National Polytechnique de Toulouse, 1977.
- 28 S. Somrani, M. Banu, M. Jemal and C. Rey, *J. Solid State Chem.*, 2005, **178**, 1337–1348.
- 29 T. Yu, J. Ye and Y. Wang, *J. Biomed. Mater. Res. - Part B Appl. Biomater.*, 2009, **90B**, 745–751.
- 30 C. Drouet, C. Largeot, G. Raimbeaux, C. Estournès, G. Dechambre, C. Combes and C. Rey, *Adv. Sci. Technol.*, 2006, **49**, 45–50.
- 31 C. Drouet, F. Bosc, M. Banu, C. Largeot, C. Combes, G. Dechambre, C. Estournès, G. Raimbeaux and C. Rey, *Powder Technol.*, 2009, **190**, 118–122.
- 32 D. Grossin, S. Rollin-Martinet, C. Estournès, F. Rossignol, E. Champion, C. Combes, C. Rey, C. Geoffroy and C. Drouet, *Acta Biomater.*, 2010, **6**, 577–585.
- 33 F. Brouillet, D. Laurencin, D. Grossin, C. Drouet, C. Estournès, G. Chevallier and C. Rey, *J. Mater. Sci. Mater. Med.*, 2015, **26**, 1–11.
- 34 C. Ortali, I. Julien, M. Vandenhende, C. Drouet and E. Champion, *J. Eur. Ceram. Soc.*, 2018, **38**, 2098–2109.
- 35 R. Orrù, R. Licheri, A. M. Locci, A. Cincotti and G. Cao, *Mater. Sci. Eng. R Reports*, 2009, **63**, 127–287.
- 36 D. Eichert, Institut National Polytechnique de Toulouse, 2001.
- 37 D. Eichert, C. Drouet, H. Sfihi, C. Rey and C. Combes, in *Biomaterials Research Advances*, ed. Jason B. Kendall, Nova Science Publishers, New York, 2007, pp. 93–143.
- 38 C. Holt, M. J. J. M. Van Kemenade, L. S. Nelson, D. W. L. Hukins, R. T. Bailey, J. E. Harries, S. S. Hasnain and P. L. De Bruyn, *Mater. Res. Bull.*, 1989, **24**, 55–62.
- 39 A. S. Posner, F. Betts and N. C. Blumenthal, *Prog. Cryst. Growth Charact.*, 1980, **3**, 49–64.
- 40 L. Berzina-Cimdina and N. Borodajenko, in *Infrared Spectroscopy - Materials Science, Engineering and Technology*, ed. T. Theophanides, InTech, Rijeka, 2012, pp. 124–148.
- 41 C. Drouet, *Biomed Res. Int.*, 2013, **2013**, 1–12.
- 42 C. Rey, C. Combes, C. Drouet and D. Grossin, in *Comprehensive Biomaterials*, eds. P. Ducheyne, W. D. Ducheyne, W. D. Grainger and C. J. Kirkpatrick, Elsevier Science, Amsterdam, 1st edn., 2011, pp. 187–221.
- 43 A. Grunenwald, C. Keyser, A. M. Sautereau, E. Crubézy, B. Ludes and C. Drouet, *J. Archaeol. Sci.*, 2014, **49**, 134–141.
- 44 M. Vignoles, G. Bonel, D. W. Holcomb and R. A. Young, *Calcif. Tissue Int.*, 1988, **43**, 33–40.
- 45 C. Rey, V. Renugopalakrishnan, B. Collins and M. J. Glimcher, *Calcif. Tissue Int.*, 1991, **49**, 251–258.
- 46 S. Cazalbou, D. Eichert, X. Ranz, C. Drouet, C. Combes, M. F. Harmand and C. Rey, *J. Mater. Sci. Mater. Med.*, 2005, **16**, 405–409.
- 47 A. Grunenwald, C. Keyser, A. M. Sautereau, E. Crubézy, B. Ludes and C. Drouet, *Anal. Bioanal. Chem.*, 2014, **406**, 4691–4704.
- 48 S. Shimoda, T. Aoba, E. C. Moreno and Y. Miake, *J. Dent. Res.*, 1990, **69**, 1731–1740.
- 49 F. Bouville and A.R. Studart, *Nat. Commun.*, 2017, **8**, article 14655 (8 pages).
- 50 Y. Doi, T. Shibusaki, Y. Moriwaki, T. Kajimoto and Y. Iwayama, *J. Biomed. Mater. Res.*, 1998, **7**,

111–122.